Electronic supplementary information

Unravelling Intrinsic Thermal Conduction Mechanism Through Phonon Transport Pathway Engineering of Long-Range Ordered Block Copolymers

Kuan Zhang, Junliang Zhang,* Jiahao An, Junwei Gu*

School of Chemistry and Chemical Engineering, Northwestern Polytechnical University, Xi'an, Shaanxi, 710072, P. R. China

*Corresponding authors: Email: junliang.zhang@nwpu.edu.cn (J. Zhang); gjw@nwpu.edu.cn (J. Gu)

Materials

4-(4-hydroxyphenyl)benzonitrile (97%), 6-chlorohexanol (98%), and 11-bromo-1-undecanol (98%), methacryloylchloride (98%), glycidyl methacrylate (GMA, 97%), 4,4'-diaminodiphenylmethane (DDM, 98%), 1,3,5-trioxane (99%), and N,N-dimethylformamide (DMF, analytical grade) were purchased from Shanghai Macklin Biochemical Co., Ltd (Shanghai, China). Triethylamine (TEA, 98%) was supplied by Aladdin Shanghai Co., Ltd. (Shanghai, China). Potassium carbonate (K_2CO_3, analytical grade), sodium bicarbonate ($NaHCO_3$, analytical grade), magnesium sulfate ($MgSO_4$, analytical grade), tetrahydrofuran (THF, analytical grade), methanol (MeOH, analytical grade), petroleum ether (analytical grade), and dichloromethane (DCM, analytical grade) were obtained from Guangdong Guanghua Science and Technology Co., Ltd. 4-cyano-4-(dodecylsulfanylthiocarbonyl)sulfanylpentanoic acid (CTA, analytical grade) was purchased from Suzhou Xinjiayuan Chemical Technology Co., Ltd. (Jiangsu, China). 1,4-dioxane (analytical grade) and 2,2'-Azobis(2-methylpropionitrile) (AIBN, analytical grade) was bought from Beijing J&K Co., Ltd. (Beijing, China).

Characterization

The molecular structure of the samples was characterized by proton and carbon nuclear magnetic resonance (^{1}H NMR and ^{13}C NMR, Bruker Avance 400 MHz, Bruker, Germany) spectroscopy. Dimethyl sulfoxide-d_6 (DMSO-d_6) or deuterated chloroform ($CDCl_3$) was used as solvents with tetramethylsilane

(TMS) as an internal standard.

Fourier transform infrared (FT-IR, Bruker Tensor II, Bruker, Germany) spectroscopy was used to characterize the functional groups of the samples. The characterization method was attenuated total internal reflectance (ATR) with the testing range of 500-4000 cm^{-1}.

Size exclusion chromatography (SEC, Waters 1515, Waters Corp., USA) was used to determine the number average molar mass (M_n), weight average molar mass (M_w), and molar mass distribution ($Đ$) of the samples using tetrahydrofuran (THF, HPLC grade) as the elution solvent at a flow rate of 1.0 mL/min. The column system was calibrated with polystyrene standards (ranging from 1000 to 10000 g/mol). The sample concentration was 0.15~0.20 wt%, and the sample was filtered through 0.45 μm Nylon syringe filters before injection.

The characteristic thermal temperatures of the samples were characterized using a differential scanning calorimetry (DSC, DSC3, Mettler-Toledo, Switzerland). The heating rate was 10°C/min and the atmosphere was nitrogen.

Wide-Angle X-ray diffraction (WAXD) patterns of the samples were tested using an WAXD (D8 Advance, Bruker, Germany) machine equipped with a Cu-targeted radiation source. The scanning speed was 10°/min with the diffraction angle of $2\theta = 5^{\circ}$ to 60°. The step size was 0.02°/step. The testing samples (powders for uncured polymers and isotropic bulk specimens for cured

polymers) were not subjected to any alignment treatment for the measurement.

Small-angle X-ray scattering (SAXS) curves of the samples were tested using a SAXS machine (Xeuss 3.0, France) equipped with a Cu-Kα targeted radiation source. The distance from the sample to the detector was 2340 mm. The scattering angle of 2θ was from 0.3° to 10°. The testing samples (powders for uncured polymers and isotropic bulk specimens for cured polymers) were not subjected to any alignment treatment for the measurement.

The glass transition temperature (T_g), melting point temperature (T_m), and curing behaviors of the samples were characterized using a differential scanning calorimetry (DSC, DSC1, Mettler-Toledo, Switzerland). The heating rate was 10°C/min and the atmosphere was nitrogen.

A hot-stage polarizing optical microscope (POM, WMP-6880, Shanghai Wumo Optical Instrument, China) was used to observe the liquid crystalline behavior of the samples with a heating rate of 10°C/min.

A thermal constant analyzer (TPS2200, Hot Disk, Sweden) was used to measure the thermal conductivity of the samples using the modular method according to the standard ISO 22007-2: 2015 at room temperature with a sample size of 20 mm × 20 mm × 3 mm. Measurements were repeated five times, and the average result of these five measurements was used for the thermal conductivity of each sample.

The FES model of the encapsulation system was built with SolidWorks, followed by a thermal performance study using ANSYS. Thermal resistance

parameters were extracted in accordance with the JESD51-2A standard, and the thickness of the encapsulation material was set at 2 mm.

The molecular dynamics model was built with Packmol software and the OPLS force field was selected to simulate liquid crystal monomers. Lammps was used to perform non-equilibrium molecular dynamics simulations (NEMD) and calculate the thermal conductivity of the system. Relaxation optimization of the geometric structure in the micro-canonical ensemble (NVE) was performed at room temperature. Heat flow was formed by a constant exchange rate of atoms in different regions, which was then stabilized into a heat flow and temperature gradient in the Z direction.

Synthesis of LCx, $PLCx_m$-*b*-$PGMA_n$, and $PLCx_{50}$-*co*-$PGMA_{50}$

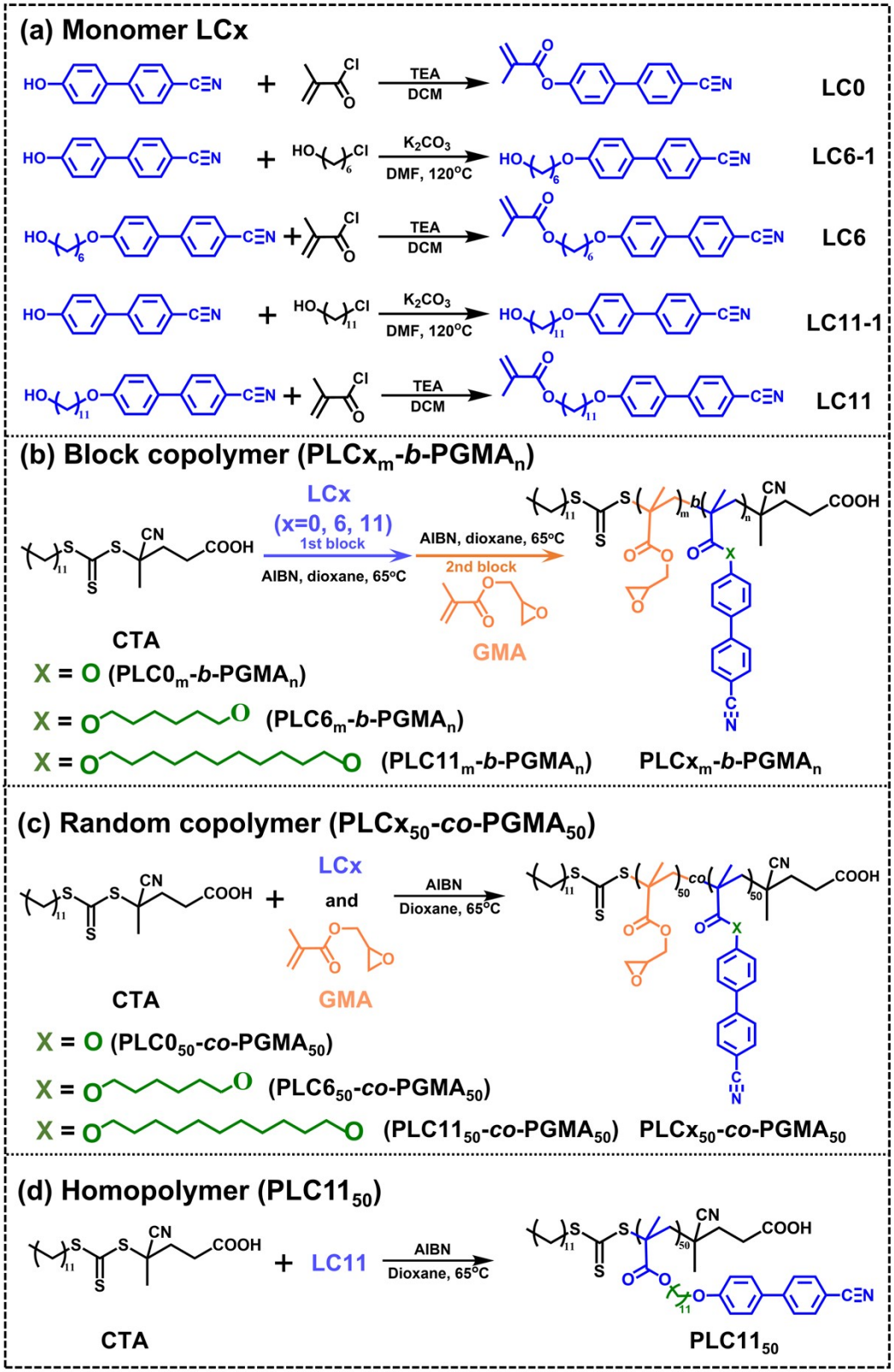

Scheme S1. Schemes for the synthesis of (a) LCx (x = 0, 6, 11), (b) $PLCx_m$-*b*-$PGMA_n$, (c) $PLCx_{50}$-*co*-$PGMA_{50}$, and (d) $PLC11_{50}$.

Synthesis of LC0: 4-(4-hydroxyphenyl)benzonitrile (5.00 g, 25.61 mmol) and TEA (3.11 g, 30.73 mmol) were dissolved in a 500 mL round bottom flask containing ultra-dry THF (100 mL). Methacryloylchloride (3.21 g, 30.73 mmol) was then dissolved in ultra-dry THF (50 mL) and added dropwise to the above solution while cooling in an ice bath. After complete addition, the mixture was allowed to react at room temperature for 24 hours, then was cooled down and washed with aqueous $NaHCO_3$ solution and water. The organic phase was dried with anhydrous $MgSO_4$ and evaporated under reduced pressure. The crude product was purified by column chromatography using DCM as eluent to obtain a white solid. The yield of the product was 86.5%. The synthetic route is shown in **Scheme S1a**.

^{1}H NMR analysis of LC0 (**Fig. 1a**, 400 MHz, $(CD_3)_2SO$, ppm): δ=7.91 (*dd*, *J*= 13, 7 Hz, –O–C_6H_4–C_6***H*****$_4$**–C≡N, **f**, **g**), δ=7.82 (*d*, *J*= 7 Hz, –O–C_6***H*****$_4$**–C_6H_4–C≡N, **e**), δ=7.32 (*d*, *J*= 7 Hz, –O–C_6***H*****$_4$**–C_6H_4–C≡N, **e**), δ= 6.31 (*s*, C***H*****$_2$**=C(CH_3)–C–, **a**), δ=5.93 (*s*, C***H*****$_2$**=C(CH_3)–C–, **b**), δ=2.02 (*s*, CH_2=C(C***H*****$_3$**)–C–, **c**). ^{13}C NMR analysis of LC0 (**Fig. 1b**, 100 MHz, $(CD_3)_2SO$, ppm): δ=165.68, 151.58, 144.23, 136.35, 135.68, 133.35, 128.79, 128.44, 128.04, 123.03, 119.39, 110.56, 18.52.

Synthesis of LC6: 4-(4-hydroxyphenyl)benzonitrile (5.00 g, 25.61 mmol), 6-chlorohexanol (5.24 g, 38.35 mmol), and K_2CO_3 (3.54 g, 25.61 mmol) were dissolved in a 500 mL round bottom flask containing DMF (200 mL). The mixture was stirred at 120^{o}C for 8 hours. After reaction, an appropriate amount

of water was added to the reaction mixture to precipitate the crude product, which was filtered and washed with water, and dried in a vacuum oven at 40°C. The obtained solid was recrystallized with methanol to obtain LC6-1 with a yield of 75.2%. Then, LC6-1 (4.00 g, 13.54 mmol) and TEA (1.64 g, 16.25 mmol) were dissolved in a 500 mL round bottom flask containing ultra-dry THF (100 mL). Then methacryloylchloride (1.70 g, 16.25 mmol) was dissolved in ultra-dry THF (50 mL) and added dropwise to the above solution while cooled in an ice bath. After complete addition, the mixture was allowed to react at room temperature for 24 hours, then was cooled down and washed with aqueous $NaHCO_3$ solution and water. The organic phase was dried with anhydrous $MgSO_4$ and evaporated under reduced pressure. The crude product was purified by column chromatography using DCM as eluent to get a white solid. The yield of the product was 68.4%. The synthetic route is shown in **Scheme S1a**.

^{1}H NMR analysis of LC6 (**Fig. 1a**, 400 MHz, $(CD_3)_2SO$, ppm): δ=7.82 (*dd*, *J*= 16, 7 Hz, –O–C_6H_4–C_6***H*****$_4$**–C≡N, **l**, **m**), δ=7.67 (*d*, *J*= 7 Hz, –O–C_6***H*****$_4$**–C_6H_4–C≡N, **k**), δ=7.02 (*d*, *J*= 7 Hz, –O–C_6***H*****$_4$**–C_6H_4–C≡N, **e**), δ= 6.01 (*s*, C***H*****$_2$**=C(CH_3)–C–, **a**), δ=5.64 (*s*, C***H*****$_2$**=C(CH_3)–C–, **b**), δ=4.09 (*t*, *J*= 5 Hz, –O–CH_2–CH_2–CH_2–CH_2–CH_2–C***H*****$_2$**–O–C_6H_4–, **i**), δ=3.99 (*t*, *J*= 5 Hz, –O–C***H*****$_2$**–CH_2–CH_2–CH_2–CH_2–CH_2–O–C_6H_4–, **d**), δ=1.87 (*s*, CH_2=C(C***H*****$_3$**)–C–, **c**), δ=1.72 (*m*, –O–CH_2–CH_2–CH_2–C***H*****$_2$**–CH_2–O–C_6H_4–, **h**) δ=1.62 (*m*, –O–CH_2–C***H*****$_2$**–CH_2–CH_2–CH_2–CH_2–O–C_6H_4–, **e**), δ=1.43 (*m*, –O–CH_2–CH_2–C***H*****$_2$**–C***H*****$_2$**–CH_2–CH_2–O–

C_6H_4–, **f**, **g**). ^{13}C NMR analysis of LC6 (**Fig. 1b**, 100 MHz, $(CD_3)_2SO$, ppm): δ=167.01, 159.81, 144.71, 136.58, 133.20, 130.70, 128.72, 127.24, 125.92,119.45, 115.49, 110.16, 67.95, 64.69, 28.98, 28.48, 25.67, 25.42, 18.45.

Synthesis of LC11: 4-(4-hydroxyphenyl)benzonitrile (5.00 g, 25.61 mmol), 11-bromo-1-undecanol (9.65 g, 38.42 mmol), and K_2CO_3 (3.54 g, 25.61 mmol) were dissolved in a 500 mL round bottom flask containing DMF (200 mL). The mixture was stirred at 120°C for 8 hours. After reaction, an appropriate amount of water was added to the reaction mixture to precipitate the crude product, which was filtered and washed with water, and dried in a vacuum drying oven at 40°C. The obtained solid was recrystallized with methanol to obtain the LC11-1 with a yield of 64.7%. Then, LC11-1 (5.00 g, 13.68 mmol) and TEA (1.66 g, 16.42 mmol) were dissolved in a 500 mL round bottom flask containing ultra-dry THF (100 mL). Then methacryloylchloride (1.72 g, 16.42 mmol) was dissolved in ultra-dry THF (50 mL) and added dropwise to the above solution while cooled in an ice bath. After complete addition, the reaction mixture was allowed to react at room temperature for 24 hours, then was cooled down and washed with aqueous $NaHCO_3$ solution and water. The organic phase was dried with anhydrous $MgSO_4$ and evaporated under reduced pressure. The crude product was purified by column chromatography using DCM as eluent to get a white solid. The yield of the product was 56.7%. The synthetic route is shown in **Scheme S1a**.

^{1}H NMR analysis of LC11 (**Fig. 1a**, 400 MHz, $(CD_3)_2SO$, ppm): δ=7.85 (*dd*, *J*= 16, 7 Hz, –O–C_6H_4–C_6***H*****$_4$**–C≡N, **k**, **l**), δ=7.69 (*d*, *J*= 7 Hz, –O–C_6***H*****$_4$**–C_6H_4–C≡N, **j**), δ=7.04 (*d*, *J*= 7 Hz, –O–C_6***H*****$_4$**–C_6H_4–C≡N, **i**), δ= 6.01 (*s*, C***H*****$_2$**=$C(CH_3)$–C–, **a**), δ=5.66 (*s*, C***H*****$_2$**=$C(CH_3)$–C–, **b**), δ=4.07 (*t*, *J*= 5 Hz, –O–CH_2–CH_2–$(CH_2)_7$–CH_2–C***H*****$_2$**–O–C_6H_4–, **h**), δ=4.01 (*t*, *J*= 5 Hz, –O–C***H*****$_2$**–CH_2–$(CH_2)_7$–CH_2–CH_2–O–C_6H_4–, **d**), δ=1.87 (*s*, CH_2=C(C***H*****$_3$**)–C–, **c**), δ=1.72 (*m*, –O–CH_2–CH_2–$(CH_2)_7$–C***H*****$_2$**–CH_2–O–C_6H_4–, **h**) δ=1.59 (*m*, –O–CH_2–C***H*****$_2$**–$(CH_2)_7$–CH_2–CH_2–O–C_6H_4–, **g**), δ=1.41, 1.25 (*m*, *m*, –O–CH_2–CH_2–(C***H*****$_2$**$)_7$–CH_2–CH_2–O–C_6H_4–, **f**). ^{13}C NMR analysis of LC11 (**Fig. 1b**, 100 MHz, $(CD_3)_2SO$, ppm): δ=167.02, 159.84, 144.74, 136.48, 133.24, 130.70, 128.76, 127.27, 125.98,119.48, 115.54, 109.55, 68.05, 64.74, 29.06, 28.52, 25.85, 18.46.

Synthesis of PLCx$_m$-*b*-PGMA$_n$ (taking PLC11$_{50}$-*b*-PGMA$_{50}$ as an example): CTA (46.56 mg, 0.12 mmol), LC11 (2.5 g, 5.77 mmol), AIBN (1.89 mg, 0.012 mmol), 1,3,5-trioxane (internal standard, 0.04 g), and 1,4-dioxane (2.88 mL) were added into a 25 mL round bottom flask. The flask was sealed with a rubber septum and degassed by bubbling nitrogen for 15 minutes and then put in an oil bath of 65^{o}C until LC11 was completely polymerized, yielding the first block polymer. Then, AIBN (2.39 mg, 0.014 mmol), GMA (0.82 g, 5.77 mmol), and 1,3,5-triazine (0.04 g, internal standard) were introduced into the reaction mixture of the first block, stirred thoroughly, sealed with a rubber septum, and bubbled with nitrogen for 15 minutes. The flask containing the reaction mixture was placed in a 65^{o}C oil bath and stirred until GMA reached

the full conversion. The reaction mixture was then diluted with an appropriate amount of dichloromethane (DCM) and added dropwise to MeOH to precipitate the polymer. The obtained solid was washed several times with MeOH and dried at 40°C for 24 hours under reduced pressure to afford PLC11$_{50}$-*b*-PGMA$_{50}$ as a light-yellow powder. The synthetic route is shown in **Scheme S1b** and the specific amounts of substrate are detailed in **Table S1-3**.

Synthesis of PLCx$_{50}$-*co*-PGMA$_{50}$ (exemplified by PLC11$_{50}$-*co*-PGMA$_{50}$): CTA (46.56 mg, 0.12 mmol), LC11 (2.50 g, 5.77 mmol), GMA (0.82 g, 5.77 mmol), AIBN (1.89 mg, 0.012 mmol), 1,3,5-trioxane (internal standard, 0.04 g), and 1,4-dioxane (5.7 mL) were added into a 25 ml round bottom flask. The flask was sealed with a rubber septum and degassed by bubbling nitrogen for 15 minutes and then put in an oil bath of 65°C until the LC11 and GMA were completely converted. The reaction mixture was then diluted with an appropriate amount of dichloromethane (DCM) and added dropwise to MeOH to precipitate the polymer. The obtained solid was washed several times with MeOH and dried at 40°C for 24 hours under reduced pressure to afford PLC11$_{50}$-*co*-PGMA$_{50}$ as a light-yellow powder. The synthetic route is shown in **Scheme S1c**, and the specific amounts of substrate are detailed in **Table S3**.

Synthesis of PLC11$_{50}$: CTA (46.56 mg, 0.12 mmol), LC11 (2.5 g, 5.77 mmol), AIBN (1.89 mg, 0.012 mmol), 1,3,5-trioxane (internal standard, 0.04 g), and 1,4-dioxane (2.88 mL) were added into a 25 mL round bottom flask. The flask was sealed with a rubber septum and degassed by bubbling nitrogen for

15 minutes and then put in an oil bath of 65°C until LC11 was completely polymerized. The reaction mixture was then diluted with an appropriate amount of dichloromethane (DCM) and added dropwise to MeOH to precipitate the polymer. The obtained solid was washed several times with MeOH and dried at 40°C for 24 hours under reduced pressure to afford $PLC11_{50}$ as a light-yellow powder. The synthetic route is shown in **Scheme S1d**

Preparation of cured $PLCx_m$-*b*-$PGMA_n$ ($B\text{-}ERx_{m\text{-}n}$)

$PLCx_m$-*b*-$PGMA_n$ and a certain amount of 4,4'-diaminodiphenylmethane (DDM, the molar ratio of amino groups in DDM to epoxy groups in $PLCx_m$-*b*-$PGMA_n$ was 1:2) were dissolved in an appropriate amount of dichloromethane (DCM) to ensure thorough mixing. DCM was then removed using a rotary evaporator and the resulting mixture was dried in an oven at 40°C for 24 hours. The dried mixture was then pressed into the desired shape and size using a mold at room temperature under 10 MPa pressure and pre-cured at the beginning temperature of the exothermic peak of the curing reaction for 2 hours, then post-cured for 2 hours at the peak temperature of the exothermic peak of the curing reaction, yielding the cured epoxies $B\text{-}ERx_{m\text{-}n}$.

FT-IR analysis of LCx (**Fig. 1c**): LC0 showed no stretching vibration peaks of methylene groups in the 3012-2798 cm^{-1} range while a stretching vibration peak of the cyano group was observed at 2227 cm^{-1}. At 1601 cm^{-1}, there was a stretching vibration peak of the carbon-carbon double bond. Compared with LC6 and LC11, the stretching vibration of the ether bond was suppressed and

showed a red shift to 1252-1149 cm^{-1}. At 1149-1050 cm^{-1}, there was a bending vibration peak of the ether bond. The stretching vibration peak of the ortho-substituted benzene ring was observed at 842-745 cm^{-1}. The peak at 3012-2798 cm^{-1} in LC6 was attributed to the stretching vibration of the methylene group. The peak at 2227 cm^{-1} was ascribed to the stretching vibration of the cyano group. The peak at 1601 cm^{-1} was attributed to the stretching vibration of the carbon-carbon double bond. The peaks at 1311-1224 cm^{-1} were attributed to the stretching vibrations of the ether bond and the peaks at 1224-1090 cm^{-1} were attributed to the bending vibrations of the ether bond. The stretching vibration peak of the para-substituted benzene ring was at 842-745 cm^{-1}. The peak of LC11 at 3012-2798 cm^{-1} was attributed to the stretching vibration of the methylene group. At 2227 cm^{-1}, the peak corresponded to the stretching vibration of the cyano group. The peak at 1601 cm^{-1} corresponded to the stretching vibration of the carbon-carbon double bond. At 1339-1217 cm^{-1}, the peaks corresponded to the stretching vibrations of the ether bond. At 1217-1090 cm^{-1}, the peaks corresponded to the bending vibrations of the ether bond. The stretching vibration peak of the para-substituted benzene ring was at 842-745 cm^{-1}. Additionally, the characteristic hydroxyl peaks at 3504-3111 cm^{-1} were absent in LC0, LC6, and LC11, indicating that the hydroxyl groups were completely substituted. The FT-IR results further confirmed the successful synthesis of LCx.

Table S1. Experimental conditions for the synthesis and characterization data of $PLC0_m$-*b*-$PGMA_n$.

	$PLC0_5$-*b*-$PGMA_{50}$		**$PLC0_{25}$-*b*-$PGMA_{50}$**		**$PLC0_{25}$-*b*-$PGMA_{25}$**		**$PLC0_{50}$-*b*-$PGMA_{50}$**		**$PLC0_{50}$-*b*-$PGMA_{25}$**		**$PLC0_{50}$-*b*-$PGMA_5$**	
	1st block	2nd block	1st block	2nd block	1st block	2nd block	1st block	2nd block	1st block	2nd block	1st block	2nd block
	LC0	GMA	LC0	GMA	LC0	GMA	LC0	GMA	LC0	GMA	LC0	GMA
$[Monomer]_0$ (mmol/mL)	2.00	2.00	2.00	2.00	2.00	1.58	2.00	1.58	2.00	0.88	2.00	0.19
$[CTA]_0/[AIBN]_{added}$	10		10		10		10		10		10	
$[AIBN]_{added}$ (mg/mL)	6.57	0.66	1.31	1.31	1.31	1.31	0.66	0.66	0.66	0.66	0.66	0.66
$[Monomer]_0/[CTA]_0$	5	50	25	50	25	25	50	50	50	25	50	5
$[m_{CTA}]_{added}$ (mg)	153.32		153.32		153.32		76.66		76.66		76.66	
$[m_{monomer}]_{added}$ (g)	0.50	2.70	2.50	2.70	2.50	1.35	2.50	1.35	2.50	0.67	2.50	0.13
$[m_{AIBN}]_{added}$ (mg)	6.24	6.24	6.24	12.47	6.24	7.89	3.12	3.94	3.12	3.53	3.12	3.20
$[V_{dioxane}]_{added}$ (mL)	0.95	6.03	4.75	2.24	4.75	0	4.75	0	4.75	0	4.75	0
monomer conversion[a]	98.60%	96.90%	97.80%	98.20%	97.90%	97.50%	98.50%	98.60%	98.90%	97.60%	98.30%	98.50%
$[DP]_{th}$[b]	4.93	48.45	24.45	49.10	24.48	24.38	49.25	49.30	49.45	24.40	49.15	4.93
$M_{n,th}$[c] (g/mol)	1700	8600	6800	13800	6800	10300	13400	20400	13400	16900	13300	14000
$M_{n,SEC}$[d] (g/mol)	/[f]	8200	7300	14400	7800	14100	15900	19800	13500	16700	13700	15400
$M_{w,SEC}$[d] (g/mol)	/[f]	9400	9400	17700	10200	16400	18600	22300	16200	18100	14800	19400
$Đ$[d]	/[f]	1.15	1.29	1.23	1.31	1.17	1.16	1.13	1.20	1.08	1.08	1.26
σ[e] (g/mol)	/[f]	3200	3900	6900	4300	5800	6400	7100	6000	4700	3800	7800
σ/M_n[e] (%)	/[f]	38.7	53.9	48.0	55.7	41.2	40.0	36.1	44.7	28.3	28.3	51.0

[a]Determined by ^{1}H NMR. [b]$[DP]_{th}$ = $[Monomer]_0/[CTA]_0$ × monomer conversion. [c]$M_{n,th}$ = $[DP]_{th}$ × M_M + M_{CTA}, M_M and M_{CTA} are the molar mass of monomer and CTA, respectively. [d]Determined by SEC using THF as an eluent with polystyrene as molar mass standards. [e] $\sigma = M_n \times \sqrt{Đ - 1}$. [f] No valid data obtained due to beyond the limitation.

Table S2. Experimental conditions for the synthesis and characterization data of $PLC6_m$-*b*-$PGMA_n$.

	$PLC6_5$-*b*-$PGMA_{50}$		**$PLC6_{25}$-*b*-$PGMA_{50}$**		**$PLC6_{25}$-*b*-$PGMA_{25}$**		**$PLC6_{50}$-*b*-$PGMA_{50}$**		**$PLC6_{50}$-*b*-$PGMA_{25}$**		**$PLC6_{50}$-*b*-$PGMA_5$**	
	1st block	2nd block	1st block	2nd block	1st block	2nd block	1st block	2nd block	1st block	2nd block	1st block	2nd block
	LC6	GMA	LC6	GMA	LC6	GMA	LC6	GMA	LC6	GMA	LC6	GMA
$[Monomer]_0$ (mmol/mL)	2.00	2.00	2.00	2.00	2.00	1.58	2.00	1.58	2.00	0.88	2.00	0.19
$[CTA]_0/[AIBN]_{added}$	10		10		10		10		10		10	
$[AIBN]_{added}$ (mg/mL)	6.57	6.57	1.31	1.31	1.31	1.31	0.66	0.66	0.66	0.66	0.66	0.66
$[Monomer]_0/[CTA]_0$	5	50	25	50	25	25	50	50	50	25	50	5
$[m_{CTA}]_{added}$ (mg)	111.08		111.08		111.08		55.54		55.54		55.54	
$[m_{monomer}]_{added}$ (g)	0.50	1.96	2.50	1.96	2.50	0.98	2.50	0.98	2.50	0.49	2.50	0.10
$[m_{AIBN}]_{added}$ (mg)	4.52	45.19	4.52	9.04	4.52	5.71	2.26	2.86	2.26	2.56	2.26	2.32
$[V_{dioxane}]_{added}$ (mL)	0.69	4.37	3.44	1.62	3.44	0	3.44	0	3.44	0	3.44	0
monomer conversion[a]	99.10%	98.60%	97.10%	97.40%	98.30%	97.90%	98.10%	98.60%	97.80%	98.20%	99.10%	98.80%
$[DP]_{th}$[b]	4.96	49.30	24.28	48.70	24.58	24.48	49.05	49.30	48.90	24.55	49.55	4.94
$M_{n,th}$[c] (g/mol)	2200	9200	9200	16100	9300	12800	18200	25200	18200	21700	18400	19100
$M_{n,SEC}$[d] (g/mol)	3600	12900	9800	18600	8400	11900	17900	24000	18800	22600	18600	19600
$M_{w,SEC}$[d] (g/mol)	4100	15200	11600	20800	9400	13600	20800	26300	23500	28200	20800	21200
$Đ$[d]	1.13	1.18	1.18	1.12	1.11	1.15	1.16	1.10	1.25	1.25	1.12	1.08
σ[e] (g/mol)	1300	5500	4200	6400	2800	4600	7200	7600	9400	11300	6400	5500
σ/M_n[e] (%)	36.1	42.4	42.4	34.6	33.2	38.7	40.0	31.6	50.0	50.0	34.6	28.3

[a]Determined by ^{1}H NMR. [b]$[DP]_{th}$ = $[Monomer]_0/[CTA]_0$ × monomer conversion. [c]$M_{n,th}$ = $[DP]_{th}$ × M_M + M_{CTA}, M_M and M_{CTA} are the molar mass of monomer and CTA, respectively. [d]Determined by SEC using THF as an eluent with polystyrene as molar mass standards. [e] $\sigma = M_n \times \sqrt{Đ - 1}$.

Table S3. Experimental conditions for the synthesis and characterization data of $PLC11_m$-*b*-$PGMA_n$ and $PLC11_{50}$-*co*-$PGMA_{50}$.

	$PLC11_5$-*b*-$PGMA_{50}$		**$PLC11_{25}$-*b*-$PGMA_{50}$**		**$PLC11_{25}$-*b*-$PGMA_{25}$**		**$PLC11_{50}$-*b*-$PGMA_{50}$**		**$PLC11_{50}$-*co*-$PGMA_{50}$**		**$PLC11_{50}$-*b*-$PGMA_{25}$**		**$PLC11_{50}$-*b*-$PGMA_5$**	
	1st block	2nd block	1st block	2nd block	1st block	2nd block	1st block	2nd block			1st block	2nd block	1st block	2nd block
	LC11	GMA	LC11	GMA	LC11	GMA	LC11	GMA	LC11	GMA	LC11	GMA	LC11	GMA
$[Monomer]_0$ (mmol/mL)	2.00	2.00	2.00	2.00	2.00	1.58	2.00	1.58	1.00	1.00	2.00	0.88	2.00	0.19
$[CTA]_0/[AIBN]_{added}$	10		10		10		10		10		10		10	
$[AIBN]_{added}$ (mg/mL)	6.57	0.66	1.31	1.31	1.31	1.31	0.66	0.66	0.33		0.66	0.66	0.66	0.66
$[Monomer]_0/[CTA]_0$	5	50	25	50	25	25	50	50	50	50	50	25	50	5
$[m_{CTA}]_{added}$ (mg)	93.11		93.11		93.11		46.56		46.54		46.56		46.56	
$[m_{monomer}]_{added}$ (g)	0.5	1.64	2.50	1.64	2.50	0.82	2.50	0.82	2.50	0.82	2.50	0.41	2.50	0.08
$[m_{AIBN}]_{added}$ (mg)	3.79	3.79	3.79	7.58	3.79	4.79	1.89	2.39	1.89		1.89	2.14	1.89	1.94
$[V_{dioxane}]_{added}$ (mL)	0.58	3.66	2.88	1.36	2.88	0	2.88	0	5.7		2.88	0	2.88	0
monomer conversion[a]	98.3%	98.8%	99.1%	98.6%	97.4%	98.5%	98.5%	99.1%	97.6%	98.5%	98.7%	98.3%	97.9%	96.4%
$[DP]_{th}$[b]	4.92	49.40	24.78	49.30	24.35	24.63	49.25	49.55	48.80	49.25	49.35	24.58	48.95	4.82
$M_{n,th}$[c] (g/mol)	2500	9600	11100	18200	11000	14500	21800	28800	28600		21800	25300	21600	22300
$M_{n,\,SEC}$[d] (g/mol)	4500	9900	12300	19400	11300	15000	21100	29600	28000		19900	24000	19600	21400
$M_{w,\,SEC}$[d] (g/mol)	5300	13800	15000	25500	12800	16500	26100	36100	33300		24900	26900	21200	25500
$Đ$[d]	1.17	1.40	1.22	1.32	1.14	1.10	1.23	1.22	1.19		1.25	1.12	1.08	1.19
σ[e] (g/mol)	1900	6300	5800	11000	4200	4700	10100	13900	12200		10000	8300	5500	9300
σ/M_n[e] (%)	41.2	63.2	46.9	56.6	37.4	31.6	48.0	46.9	43.6		50.0	34.6	28.3	43.6

[a]Determined by ^{1}H NMR. [b]$[DP]_{th}$ = $[Monomer]_0/[CTA]_0$ × monomer conversion. [c]$M_{n,th}$ = $[DP]_{th}$ × M_M + M_{CTA}, M_M and M_{CTA} are the molar mass of monomer and CTA, respectively. [d]Determined by SEC using THF as an eluent with polystyrene as molar mass standards. [e] $\sigma = M_n \times \sqrt{Đ - 1}$.

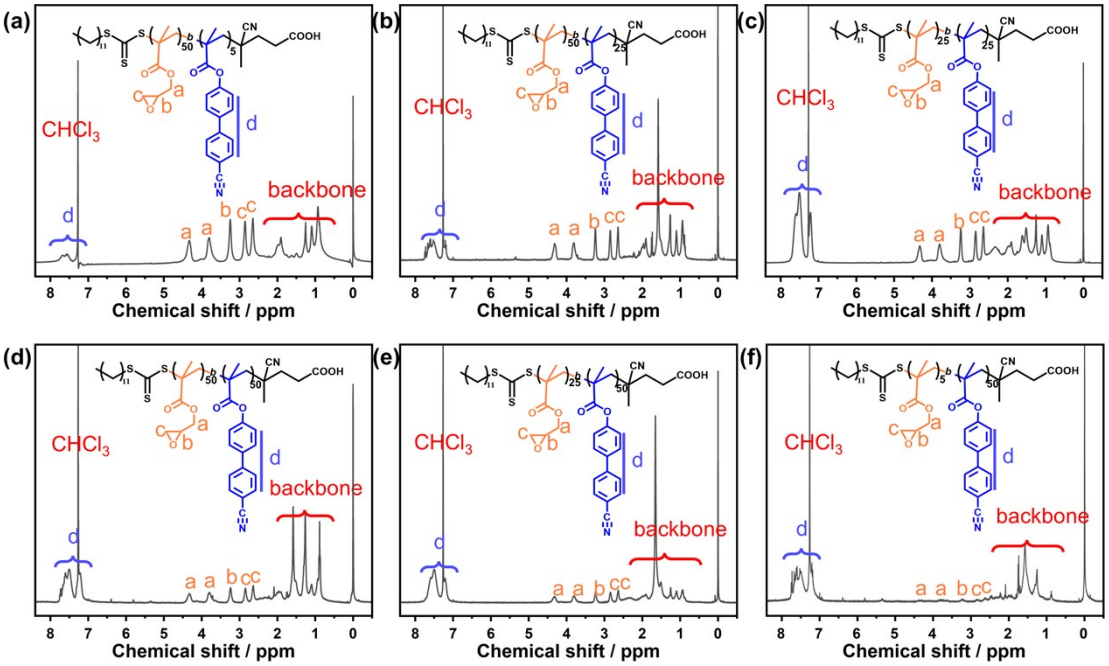

Fig. S1. ^{1}H NMR spectra of (a) PLC0$_5$-*b*-PGMA$_{50}$, (b) PLC0$_{25}$-*b*-PGMA$_{50}$, (c) PLC0$_{25}$-*b*-PGMA$_{25}$, (d) PLC0$_{50}$-*b*-PGMA$_{50}$, (e) PLC0$_{50}$-*b*-PGMA$_{25}$, and (f) PLC0$_{50}$-*b*-PGMA$_5$.

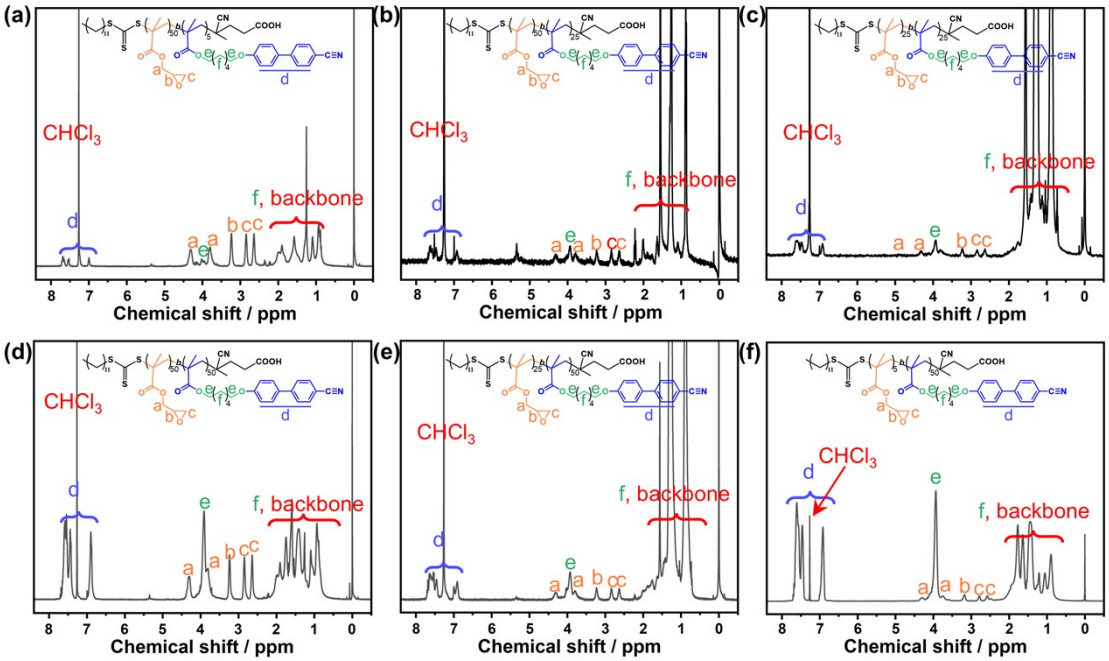

Fig. S2. ^{1}H NMR spectra of (a) PLC6$_5$-*b*-PGMA$_{50}$, (b) PLC6$_{25}$-*b*-PGMA$_{50}$, (c) PLC6$_{25}$-*b*-PGMA$_{25}$, (d) PLC6$_{50}$-*b*-PGMA$_{50}$, (e) PLC6$_{50}$-*b*-PGMA$_{25}$, and (f) PLC6$_{50}$-*b*-PGMA$_5$.

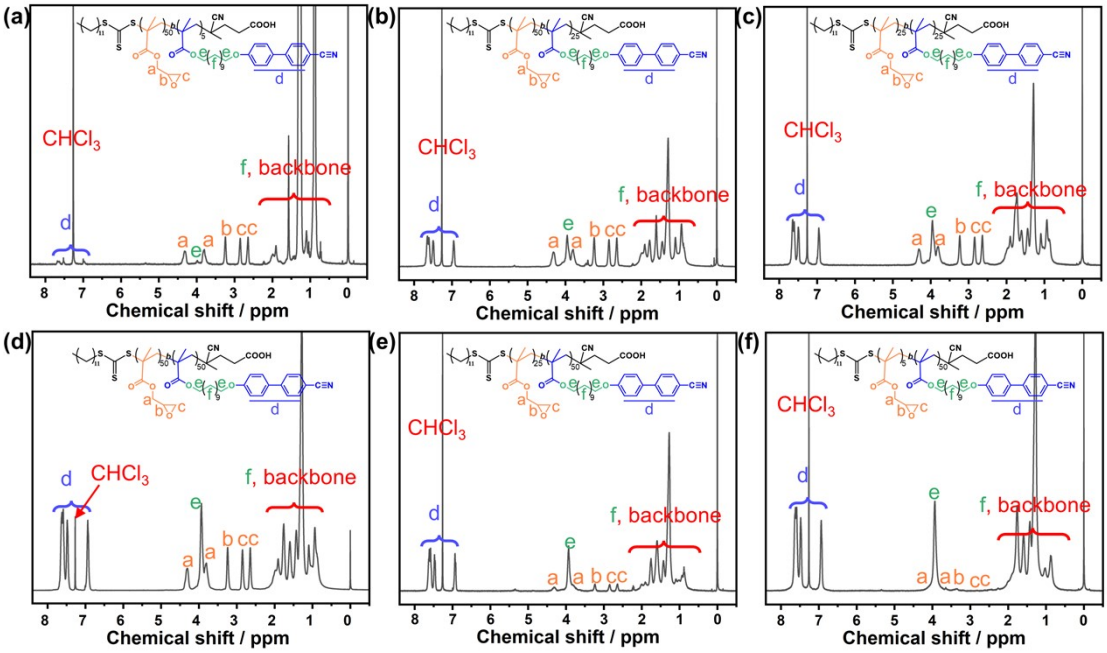

Fig. S3. ^{1}H NMR spectra of (a) PLC11$_5$-*b*-PGMA$_{50}$, (b) PLC11$_{25}$-*b*-PGMA$_{50}$, (c) PLC11$_{25}$-*b*-PGMA$_{25}$, (d) PLC11$_{50}$-*b*-PGMA$_{50}$, (e) PLC11$_{50}$-*b*-PGMA$_{25}$, and (f) PLC11$_{50}$-*b*-PGMA$_5$.

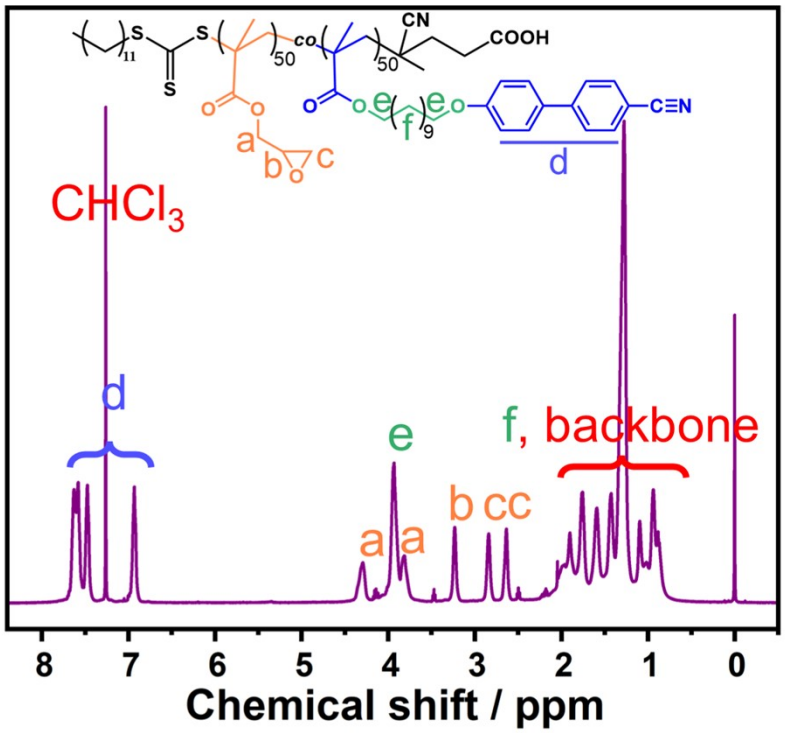

Fig. S4. ^{1}H NMR spectra of PLC11$_{50}$-*co*-PGMA$_{50}$.

^{1}H NMR analysis of PLCx$_m$-*b*-PGMA$_n$ and PLCx$_{50}$-*co*-PGMA$_{50}$ (**Fig. 1h** and **Fig. S1-4**, 400 MHz, $CDCl_3$, exemplified by PLC11$_{50}$-*b*-PGMA$_{50}$): The peaks at 7.58, 7.47, and 6.92 ppm were assigned to protons in the benzene rings of

LC11. The peaks at 4.29, 3.82, 3.24, 2.85, and 2.64 ppm were attributed to protons of epoxy groups. The peaks at 3.94 and 1.93-0.93 ppm were ascribed to protons of the flexible chain segment $(\text{-CH}_2\text{-})_{11}$ and main chain of the polymer. ^{13}C NMR analysis of PLCx$_m$-*b*-PGMA$_n$ and PLCx$_{50}$-*co*-PGMA$_{50}$ (**Fig. 1i**, 100 MHz, $CDCl_3$, exemplified by PLC11$_{50}$-*b*-PGMA$_{50}$): The peak at 159.7 ppm was attributed to the carbonyl groups in GMA and LC11. The peaks at 145.1-110.1 ppm were corresponded to the carbon atoms in the benzene rings of the biphenyl structure in LC11. The peaks at 68.1, 49.0, and 44.7 ppm were assigned to the three carbon atoms of the epoxy group in GMA. The peak at 65.9 ppm belonged to the carbon atom of the flexible chain segment $(\text{-CH}_2\text{-})_{11}$. The peaks at 29.7 to 16.6 ppm belonged to the carbon atoms of the polymer main chain.

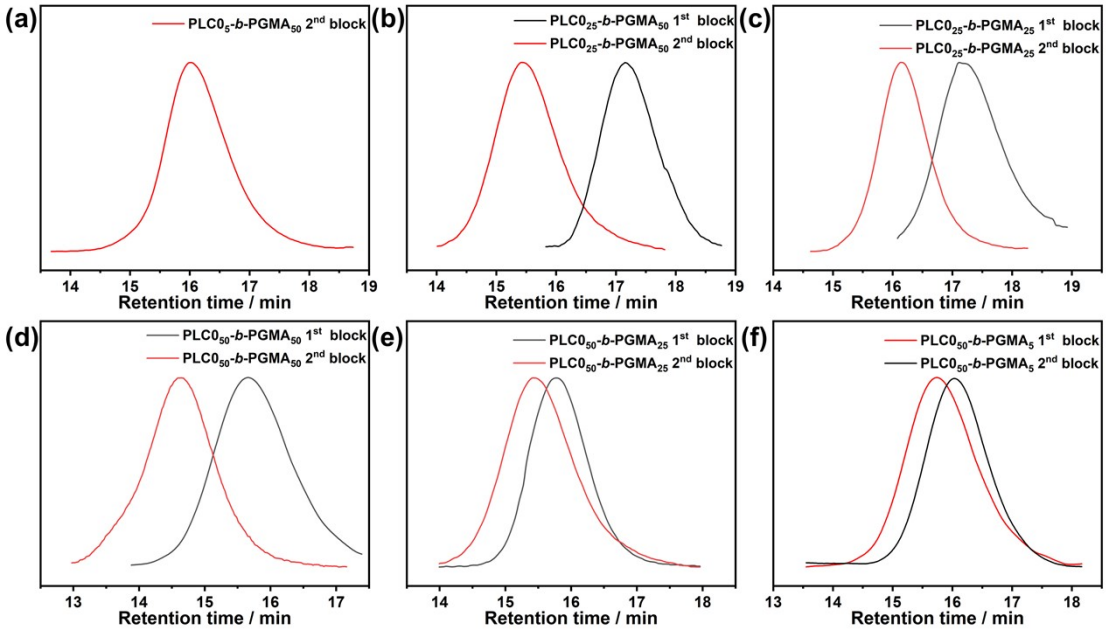

Fig. S5. SEC curves of (a) PLC0$_5$-*b*-PGMA$_{50}$ (No valid data for the block obtained due to beyond the limitation), (b) PLC0$_{25}$-*b*-PGMA$_{50}$, (c) PLC0$_{25}$-*b*-PGMA$_{25}$, (d) PLC0$_{50}$-*b*-PGMA$_{50}$, (e) PLC0$_{50}$-*b*-PGMA$_{25}$, and (f) PLC0$_{50}$-*b*-PGMA$_5$.

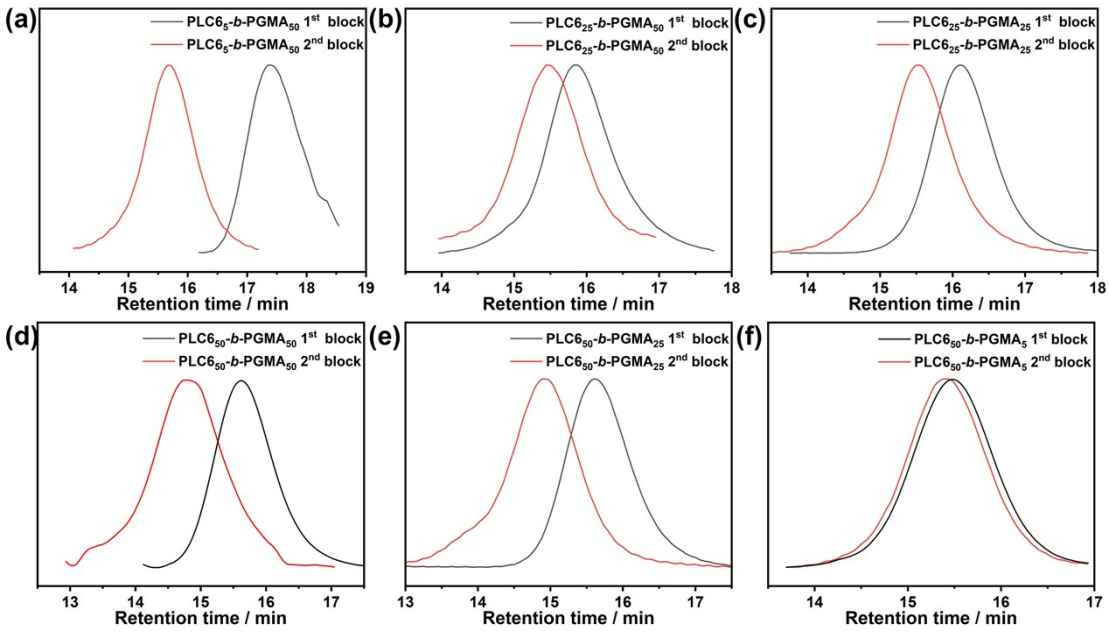

Fig. S6. SEC curves of (a) PLC6$_5$-*b*-PGMA$_{50}$, (b) PLC6$_{25}$-*b*-PGMA$_{50}$, (c) PLC6$_{25}$-*b*-PGMA$_{25}$, (d) PLC6$_{50}$-*b*-PGMA$_{50}$, (e) PLC6$_{50}$-*b*-PGMA$_{25}$, and (f) PLC6$_{50}$-*b*-PGMA$_5$.

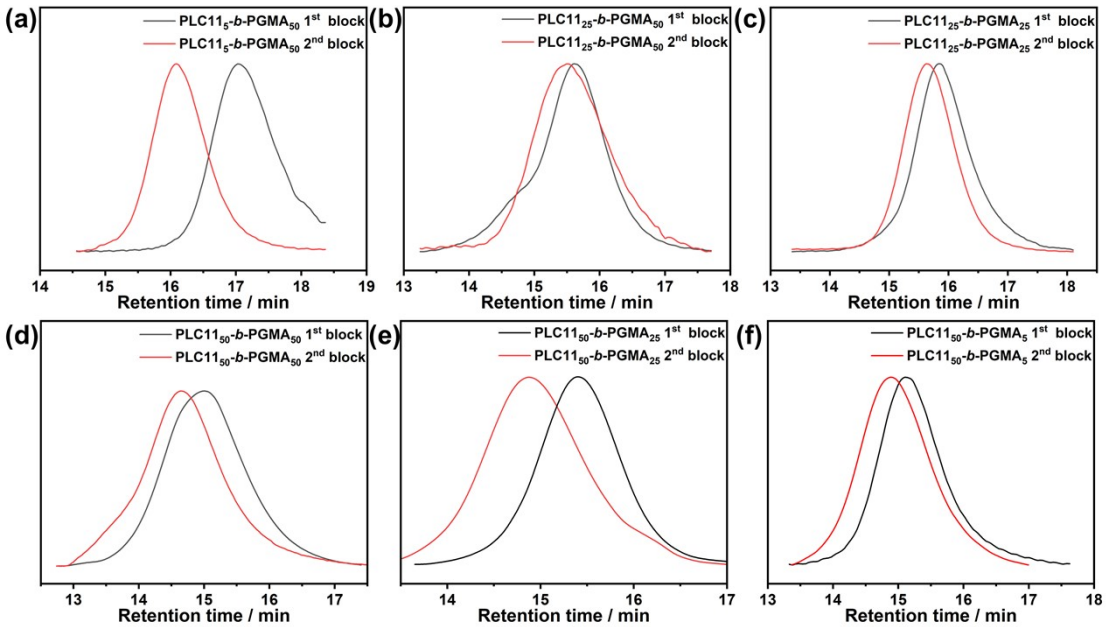

Fig. S7. SEC curves of (a) PLC11$_5$-*b*-PGMA$_{50}$, (b) PLC11$_{25}$-*b*-PGMA$_{50}$, (c) PLC11$_{25}$-*b*-PGMA$_{25}$, (d) PLC11$_{50}$-*b*-PGMA$_{50}$, (e) PLC11$_{50}$-*b*-PGMA$_{25}$, and (f) PLC11$_{50}$-*b*-PGMA$_5$.

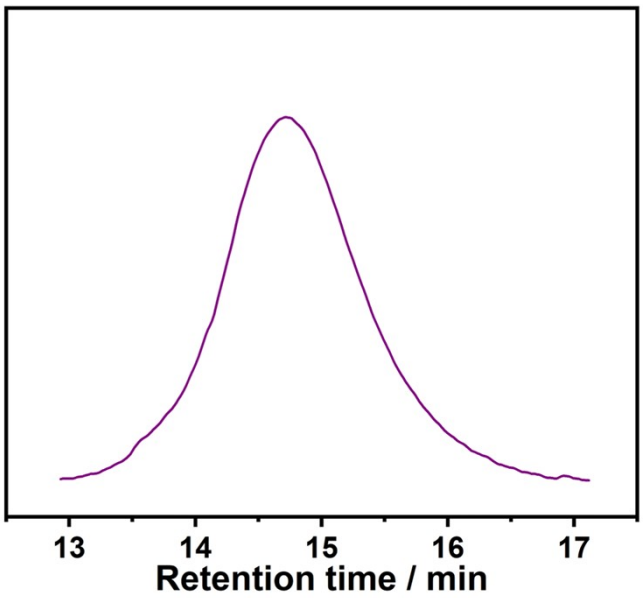

Fig. S8. SEC curve of PLCx$_{50}$-*co*-PGMA$_{50}$ (exemplified by PLC11$_{50}$-*co*-PGMA$_{50}$).

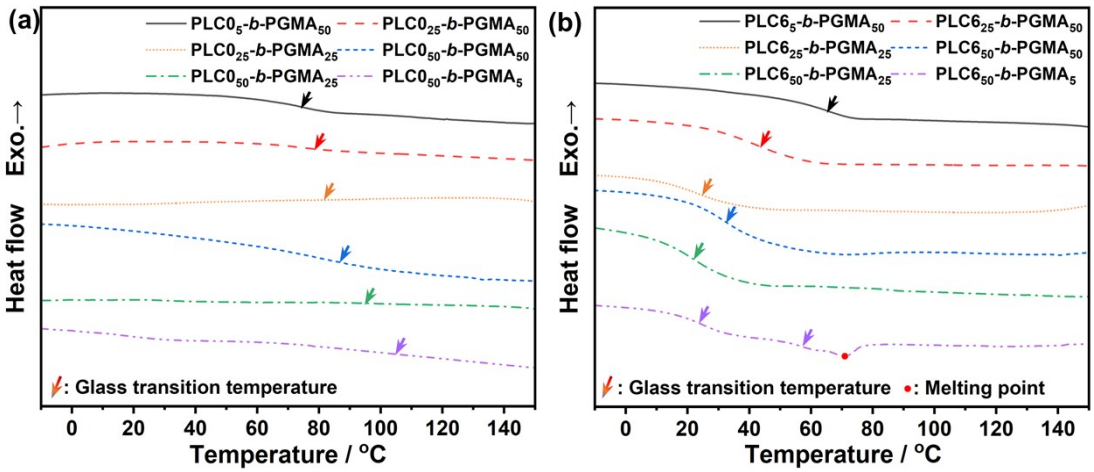

Fig. S9. DSC curves of (a) PLC0$_m$-*b*-PGMA$_n$ and (b) PLC6$_m$-*b*-PGMA$_n$.

Flory-Fox equation

$$T_g = T_g(\infty) - \frac{K}{M_n} \qquad \textbf{(Eq. S1)}$$

where $T_g(\infty)$ is the glass transition temperature of the polymer when the molecular weight is infinite, *K* is the characteristic constant for each polymer, and M_n is the number average molecular weight.

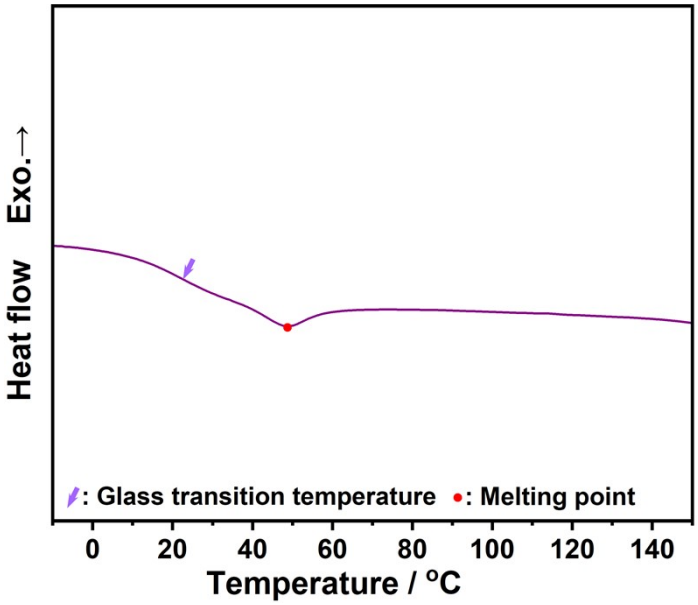

Fig. S10. DSC curve of PLC11$_{50}$-*co*-PGMA$_{50}$.

Table S4. DSC data of PLCx$_m$-*b*-PGMA$_n$ and PLC11$_{50}$-*co*-PGMA$_{50}$.

Sample	T_g / °C		T_m / °C	ΔH_m[a] / J·g^{-1}
	T_{g1}	T_{g2}		
PLC0$_5$-*b*-PGMA$_{50}$	74.3	/	/	/
PLC0$_{25}$-*b*-PGMA$_{50}$	78.5	/	/	/
PLC0$_{25}$-*b*-PGMA$_{25}$	81.7	/	/	/
PLC0$_{50}$-*b*-PGMA$_{50}$	86.4	/	/	/
PLC0$_{50}$-*b*-PGMA$_{25}$	94.6	/	/	/
PLC0$_{50}$-*b*-PGMA$_5$	104.5	/	/	/
PLC6$_5$-*b*-PGMA$_{50}$	65.8	/	/	/
PLC6$_{25}$-*b*-PGMA$_{50}$	43.4	/	/	/
PLC6$_{25}$-*b*-PGMA$_{25}$	24.4	/	/	/
PLC6$_{50}$-*b*-PGMA$_{50}$	31.5	/	/	/
PLC6$_{50}$-*b*-PGMA$_{25}$	21.7	/	/	/
PLC6$_{50}$-*b*-PGMA$_5$	23.7	57.2	71.0	0.77
PLC11$_5$-*b*-PGMA$_{50}$	60.7	/	/	/
PLC11$_{25}$-*b*-PGMA$_{50}$	15.6	33.3	77.8	1.62
PLC11$_{25}$-*b*-PGMA$_{25}$	13.1	30.4	67.6	2.20
PLC11$_{50}$-*b*-PGMA$_{50}$	15.9	36.4	96.5	3.01
PLC11$_{50}$-*co*-PGMA$_{50}$	22.3	/	48.4	2.56
PLC11$_{50}$-*b*-PGMA$_{25}$	8.4	30.1	79.7	5.05
PLC11$_{50}$-*b*-PGMA$_5$	7.6	29.5	84.6	8.91

[a]Obtained from DSC, $\Delta H = \frac{\int_{T_2}^{T_1} (\frac{dQ}{dt}) dt}{m}$, where T_1 and T_2 are the start and end temperatures of the characteristic peak, $\frac{dQ}{dt}$ is the heat flow, and m is the sample mass. Calculate ΔH_f, ΔH_c, ΔH_{cp} using this method.

Curing of PLCx$_m$-*b*-PGMA$_n$: To achieve an ordered microstructure, a pre-curing and post-curing process was employed. Specifically, the polymer was pre-cured for 2 hours at the beginning temperature of the curing exothermic peak and post-cured for 2 hours at the peak temperature of the curing exothermic peak (**Fig. S11**). DSC curves of B-ERx$_{m-n}$ and R-ER11$_{m-n}$ showed no exothermic peaks indicative of curing reactions (**Fig. S12-13**). In FT-IR spectra (**Fig. S14-15**), the characteristic peaks of the epoxy groups at 913 cm^{-1} in B-ERx$_{m-n}$ and R-ERx$_{m-n}$ have completely disappeared while a secondary hydroxyl peak at 3374 cm^{-1} appeared, which was generated by epoxy ring-opening, confirming the epoxy groups have completely cured. Notably, R-ER11$_{50-50}$ formed by curing the random copolymer PLC11$_{50}$-*co*-PGMA$_{50}$ (melting point temperature (T_m) = 48.4^{o}C, ΔH_m = 2.56 J/g) no longer exhibited a crystalline melting peak (**Fig. S13**), while B-ER11$_{50-50}$ cured by PLC11$_{50}$-*b*-PGMA$_{50}$ (T_m = 96.5^{o}C, ΔH_m = 3.01 J/g) still exhibited distinct crystalline melting peaks (T_m = 104.6^{o}C, ΔH_m = 2.84 J/g), indicating that the block copolymer effectively retained the crystalline structure of the polymer during curing.

The detailed curing processes of the polymers were as following: 70^{o}C/2 hours + 125^{o}C/2 hours for PLC0$_5$-*b*-PGMA$_{50}$; 80^{o}C/2 hours + 160^{o}C/2 hours for

$PLC0_{25}$-*b*-$PGMA_{50}$; 75°C/2 hours + 160°C/2 hours for $PLC0_{25}$-*b*-$PGMA_{25}$; 80°C/2 hours + 155°C/2 hours for $PLC0_{50}$-*b*-$PGMA_{50}$; 95°C/2 hours + 150°C/2 hours for $PLC0_{50}$-*b*-$PGMA_{25}$; 125°C/2 hours + 160°C/2 hours for $PLC0_{50}$-*b*-$PGMA_5$; 70°C/2 hours + 140°C/2 hours for $PLC6_5$-*b*-$PGMA_{50}$; 70°C/2 hours + 145°C/2 hours for $PLC6_{25}$-*b*-$PGMA_{50}$; 100°C/2 hours + 170°C/2 hours for $PLC6_{25}$-*b*-$PGMA_{25}$; 90°C/2 hours + 170°C/2 hours for $PLC6_{50}$-*b*-$PGMA_{50}$; 95°C/2 hours + 135°C/2 hours for $PLC6_{50}$-*b*-$PGMA_{25}$; 100°C/2 hours + 175°C/2 hours for $PLC6_{50}$-*b*-$PGMA_5$; 60°C/2 hours + 125°C/2 hours for $PLC11_5$-*b*-$PGMA_{50}$; 80°C/2 hours + 145°C/2 hours for $PLC11_{25}$-*b*-$PGMA_{50}$; 100°C/2 hours + 175°C/2 hours for $PLC11_{25}$-*b*-$PGMA_{25}$; was as following: 95°C/2 hours + 170°C/2 hours for $PLC11_{50}$-*b*-$PGMA_{50}$; 70°C/2 hours + 170°C/2 hours for $PLC11_{50}$-*co*-$PGMA_{50}$; 110°C/2 hours + 180°C/2 hours for $PLC11_{50}$-*b*-$PGMA_{25}$; 110°C/2 hours + 170°C/2 hours for $PLC11_{50}$-*b*-$PGMA_5$.

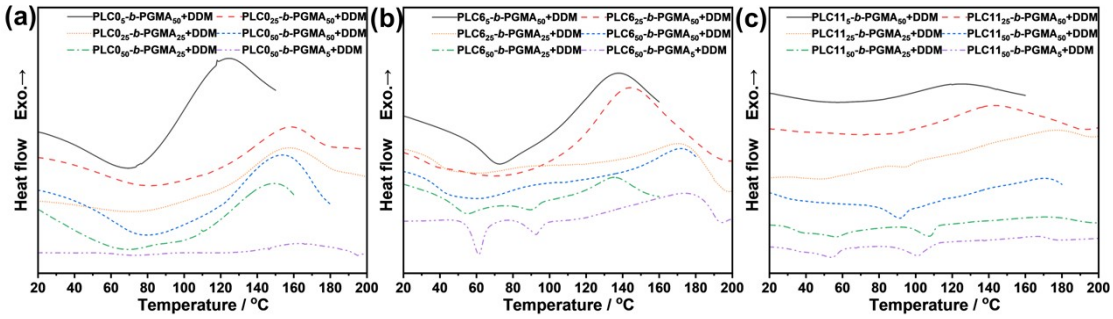

Fig. S11. DSC curves of the curing process of (a) $PLC0_m$-*b*-$PGMA_n$, (b) $PLC6_m$-*b*-$PGMA_n$, and (c) $PLC11_m$-*b*-$PGMA_n$ with DDM.

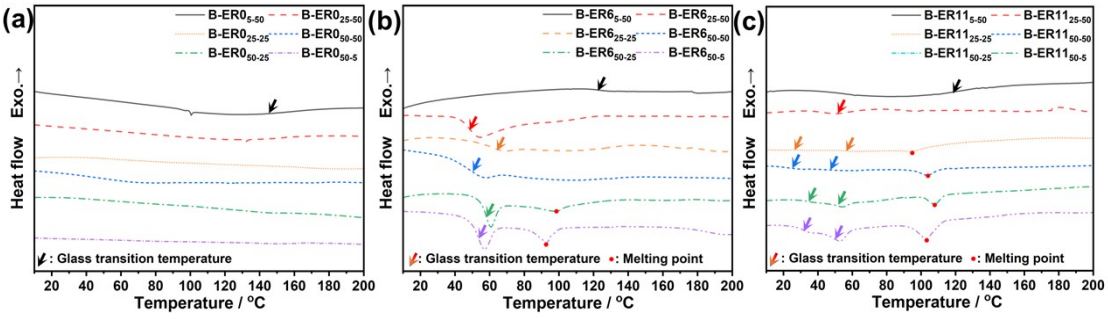

Fig. S12. DSC curves of (a) B-ER0$_{m\text{-}n}$, (b) B-ER6$_{m\text{-}n}$, and (c) B-ER11$_{m\text{-}n}$.

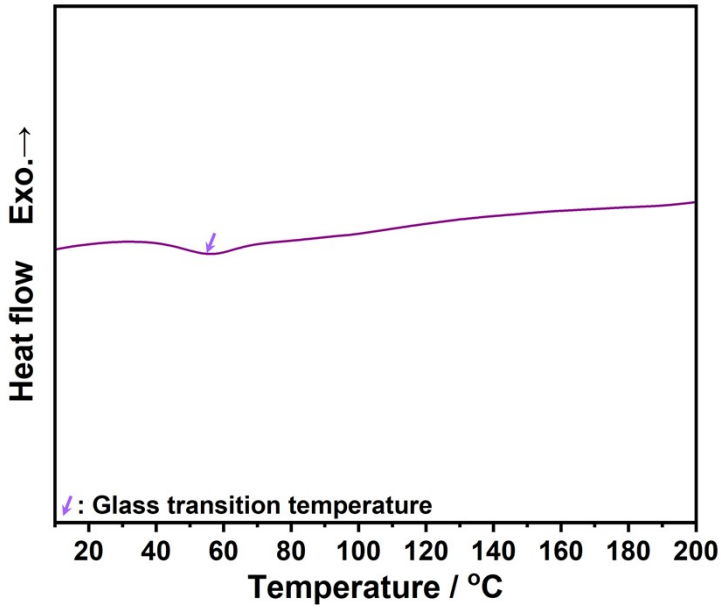

Fig. S13. DSC curve of R-ER11$_{50\text{-}50}$.

Table S5. DSC data of B-ERx$_{m\text{-}n}$ and R-ER11$_{50\text{-}50}$.

Sample	T_g / °C		T_m / °C	ΔH_m[a] / J·g^{-1}
	T_{g1}	T_{g2}		
B-ER0$_{5\text{-}50}$	145.2	/	/	/
B-ER0$_{25\text{-}50}$	/	/	/	/
B-ER0$_{25\text{-}25}$	/	/	/	/
B-ER0$_{50\text{-}50}$	/	/	/	/
B-ER0$_{50\text{-}25}$	/	/	/	/
B-ER0$_{50\text{-}5}$	/	/	/	/
B-ER6$_{5\text{-}50}$	122.3	/	/	/
B-ER6$_{25\text{-}50}$	48.7	/	/	/
B-ER6$_{25\text{-}25}$	64.8	/	/	/
B-ER6$_{50\text{-}50}$	50.3	/	/	/
B-ER6$_{50\text{-}25}$	58.2	/	98.6	1.63
B-ER6$_{50\text{-}5}$	53.5	/	92.7	2.99
B-ER11$_{5\text{-}50}$	118.5	/	/	/
B-ER11$_{25\text{-}50}$	52.0	/	/	/
B-ER11$_{25\text{-}25}$	26.6	56.8	94.4	0.37
B-ER11$_{50\text{-}50}$	25.8	47.7	104.6	2.84
R-ER11$_{50\text{-}50}$	55.4	/	/	/
B-ER11$_{50\text{-}25}$	34.6	51.7	108.4	3.10

B-ER11$_{50\text{-}5}$	32.0	50.4	103.3	6.66

[a]Obtained from DSC, $\Delta H = \frac{\int_{T_2}^{T_1} (\frac{dQ}{dt}) dt}{m}$, where T_1 and T_2 are the start and end temperatures of the characteristic peak, $\frac{dQ}{dt}$ is the heat flow, and m is the sample mass. Calculate ΔH_f, ΔH_c, ΔH_{cp} using this method.

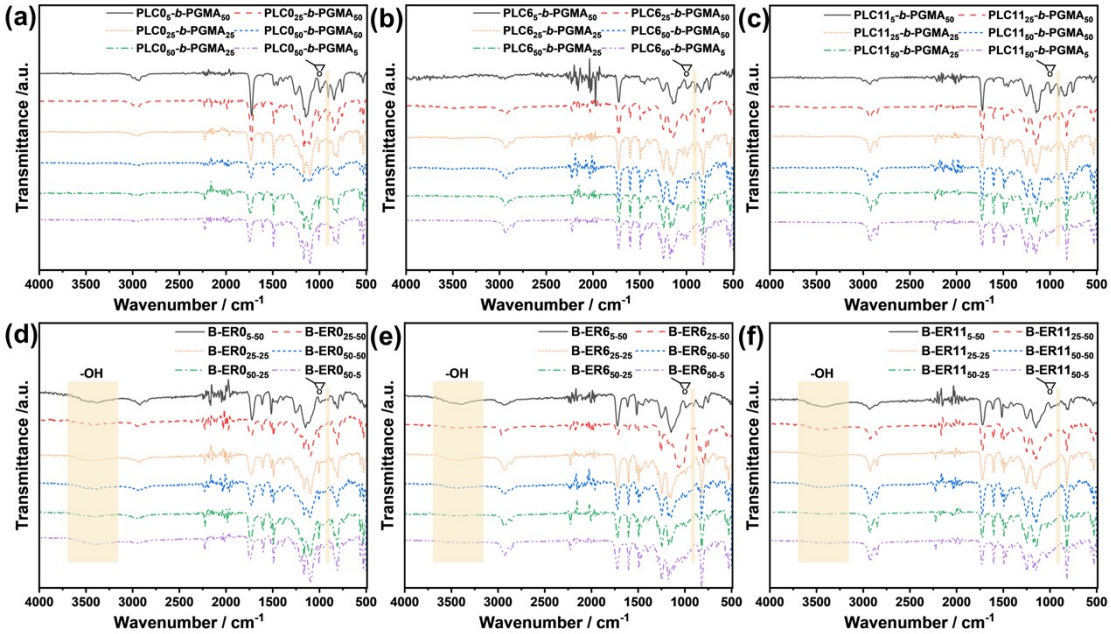

Fig. S14. FT-IR spectra of (a) PLC0$_m$-*b*-PGMA$_n$, (b) PLC6$_m$-*b*-PGMA$_n$, (c) PLC11$_m$-*b*-PGMA$_n$, (d) B-ER0$_{m\text{-}n}$, (e) B-ER6$_{m\text{-}n}$, and (f) B-ER11$_{m\text{-}n}$.

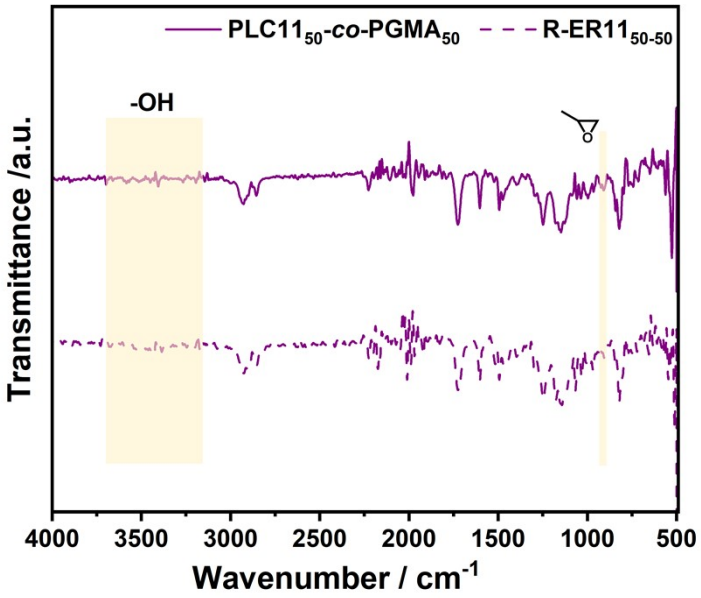

Fig. S15. FT-IR spectra of PLC11$_{50}$-*co*-PGMA$_{50}$ and R-ER11$_{50\text{-}50}$.

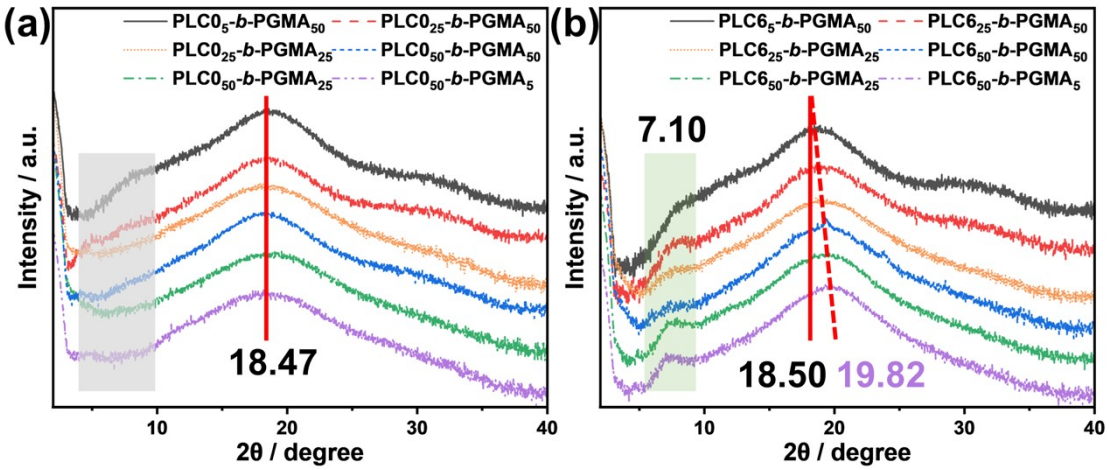

Fig. S16. WAXD curves of (a) PLC0$_m$-*b*-PGMA$_n$ and (b) PLC6$_m$-*b*-PGMA$_n$.

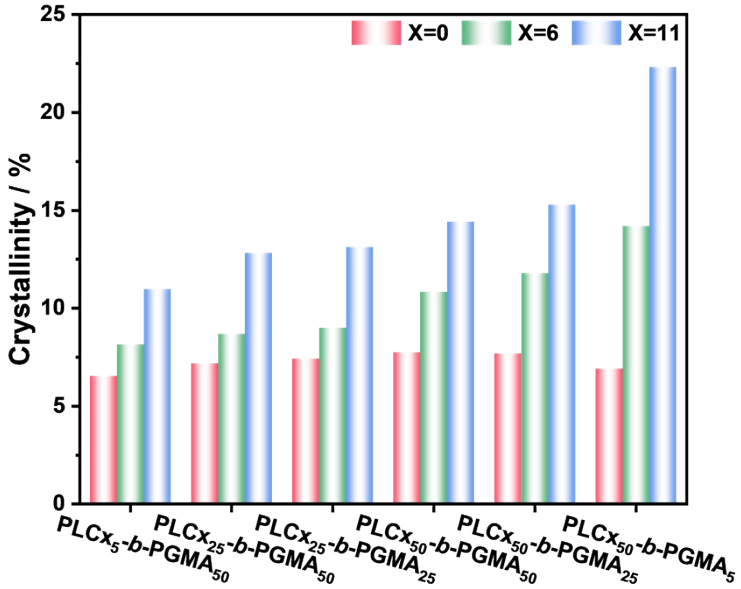

Fig. S17. Crystallinity of PLCx$_m$-*b*-PGMA$_n$.

Table S6. Crystalline grain structure and λ values for PLCx$_m$-*b*-PGMA$_n$, PLC11$_{50}$-*co*-PGMA$_{50}$, and PLC11$_{50}$

Samples	d_1[a] / Å	d_2[a] / Å	λ / W/(m·K)
PLC0$_5$-*b*-PGMA$_{50}$	4.80	/	0.20 ± 0.0031
PLC0$_{25}$-*b*-PGMA$_{50}$	4.80	/	0.19 ± 0.0043
PLC0$_{25}$-*b*-PGMA$_{25}$	4.80	/	0.20 ± 0.0044
PLC0$_{50}$-*b*-PGMA$_{50}$	4.80	/	0.21 ± 0.0036
PLC0$_{50}$-*b*-PGMA$_{25}$	4.80	/	0.21 ± 0.0041
PLC0$_{50}$-*b*-PGMA$_5$	4.80	/	0.22 ± 0.0036
PLC6$_5$-*b*-PGMA$_{50}$	4.79	11.37	0.24 ± 0.0046
PLC6$_{25}$-*b*-PGMA$_{50}$	4.68	12.44	0.22 ± 0.0032

Table S6. Crystalline grain structure and λ values for PLCx$_m$-*b*-PGMA$_n$, PLC11$_{50}$-*co*-PGMA$_{50}$, and PLC11$_{50}$ (Continued).

Samples	d_1[a] / Å	d_2[a] / Å	λ / W/(m·K)
PLC6$_{25}$-*b*-PGMA$_{25}$	4.61	12.44	0.23 ± 0.0051
PLC6$_{50}$-*b*-PGMA$_{50}$	4.57	12.44	0.23 ± 0.0036
PLC6$_{50}$-*b*-PGMA$_{25}$	4.53	12.44	0.24 ± 0.0028
PLC6$_{50}$-*b*-PGMA$_5$	4.47	12.44	0.26 ± 0.0042
PLC11$_5$-*b*-PGMA$_{50}$	4.77	11.45	0.25 ± 0.0039
PLC11$_{25}$-*b*-PGMA$_{50}$	4.53	17.14	0.23 ± 0.0044
PLC11$_{25}$-*b*-PGMA$_{25}$	4.49	17.14	0.27 ± 0.0031
PLC11$_{50}$-*b*-PGMA$_{50}$	4.43	17.14	0.27 ± 0.0042
PLC11$_{50}$-*b*-PGMA$_{25}$	4.42	17.14	0.25 ± 0.0051
PLC11$_{50}$-*co*-PGMA$_{50}$	4.49	17.14	0.22 ± 0.0038
PLC11$_{50}$-*b*-PGMA$_5$	4.40	17.14	0.29 ± 0.0031
PLC11$_{50}$	4.38	15.94	0.33 ± 0.0034

[a]Determined based on the WAXD results.

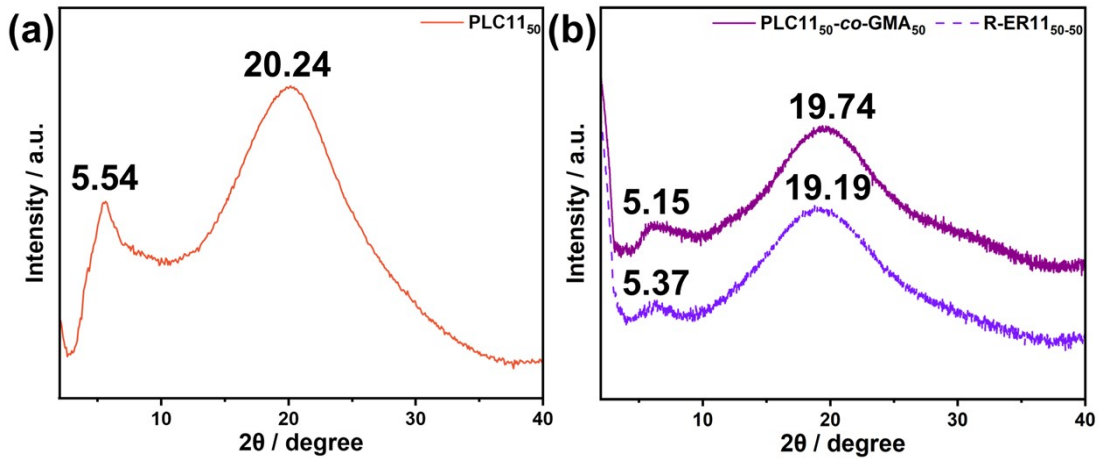

Fig. S18. WAXD curves of (a) PLC11$_{50}$ and (b) PLC11$_{50}$-*co*-PGMA$_{50}$ and R-ER11$_{50-50}$.

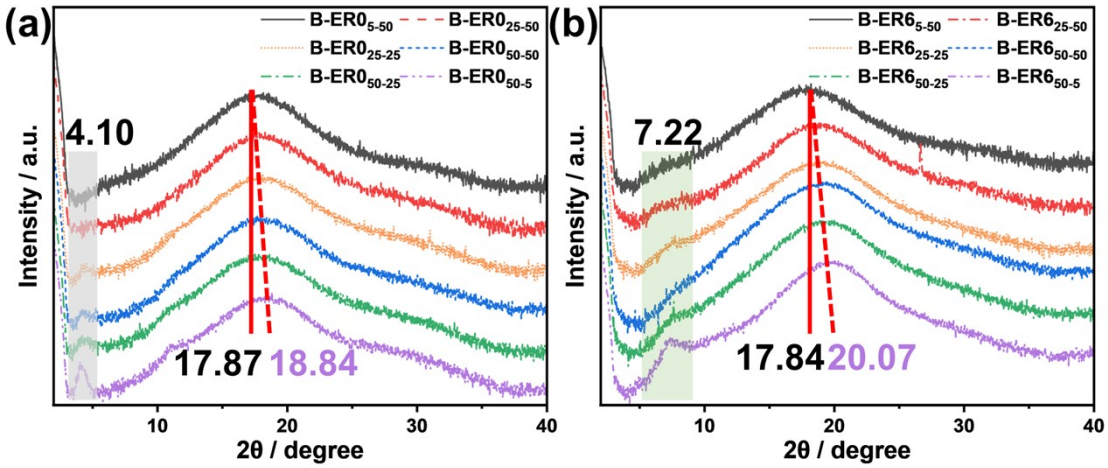

Fig. S19. WAXD curves of (a) B-ER0$_{m-n}$ and (b) B-ER6$_{m-n}$.

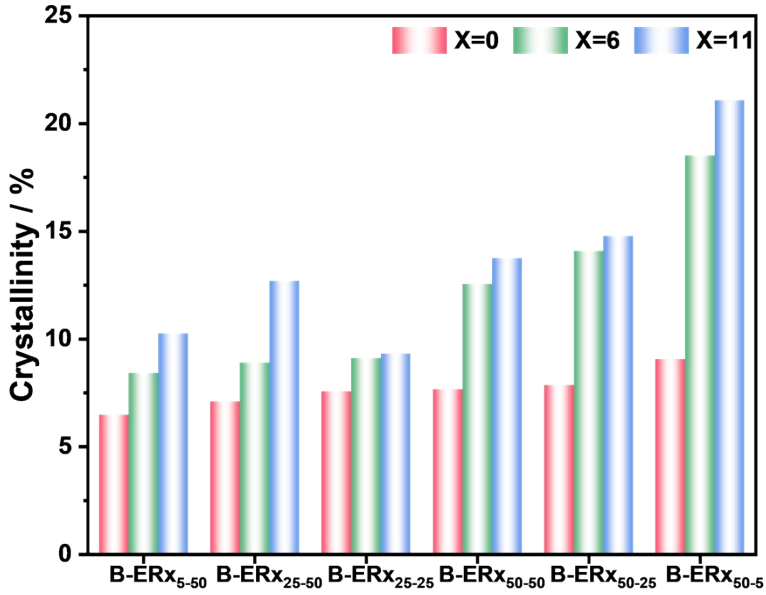

Fig. S20. Crystallinity of B-ERx$_{m-n}$.

Table S7. Crystalline grain structure and λ values for B-ERx$_{m-n}$ and R-ER11$_{50-50}$.

Samples	d_1[a] / Å	d_2[a] / Å	λ / W/(m·K)
B-ER0$_{5-50}$	4.96	/	0.26 ± 0.0062
B-ER0$_{25-50}$	4.95	/	0.27 ± 0.0037
B-ER0$_{25-25}$	4.86	21.53	0.27 ± 0.0045
B-ER0$_{50-50}$	4.81	21.53	0.27 ± 0.0022
B-ER0$_{50-25}$	4.78	21.53	0.28 ± 0.0051
B-ER0$_{50-5}$	4.71	21.53	0.30 ± 0.0054
B-ER6$_{5-50}$	4.97	/	0.29 ± 0.0018
B-ER6$_{25-50}$	4.74	/	0.32 ± 0.0024

Table S7. Crystalline grain structure and λ values for for B-ERx$_{m-n}$ and R-ER11$_{50-50}$ (Continued).

Samples	d_1[a] / Å	d_2[a] / Å	λ / W/(m·K)
B-ER6$_{25-25}$	4.64	/	0.28 ± 0.0039
B-ER6$_{50-50}$	4.58	/	0.33 ± 0.0037
B-ER6$_{50-25}$	4.48	12.23	0.34 ± 0.0028
B-ER6$_{50-5}$	4.42	12.23	0.36 ± 0.0036
B-ER11$_{5-50}$	4.95	16.44	0.32 ± 0.0041
B-ER11$_{25-50}$	4.72	16.44	0.33 ± 0.0023
B-ER11$_{25-25}$	4.56	16.44	0.30 ± 0.0029
B-ER11$_{50-50}$	4.51	16.44	0.37 ± 0.0052
R-ER11$_{50-50}$	4.62	16.44	0.29 ± 0.0032
B-ER11$_{50-25}$	4.41	16.44	0.35 ± 0.0026
B-ER11$_{50-5}$	4.38	16.44	0.39 ± 0.0036

[a]Determined based on the WAXD results.

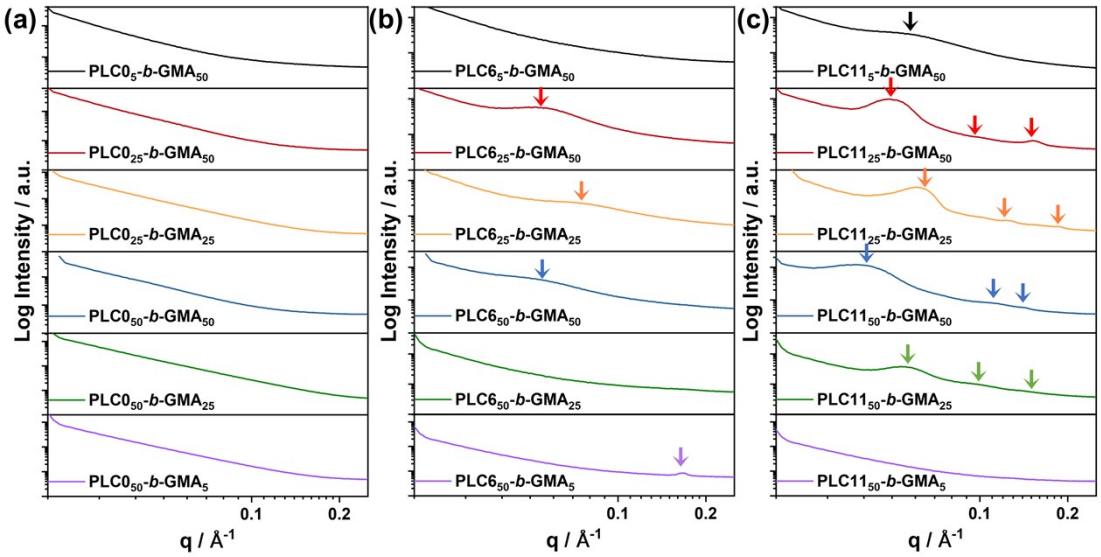

Fig. S21. SAXS curves of (a) PLC0$_m$-*b*-PGMA$_n$, (b) PLC6$_m$-*b*-PGMA$_n$, and (c) PLC11$_m$-*b*-PGMA$_n$.

Table S8. SAXS peak positions for PLCx$_m$-*b*-PGMA$_n$ and B-ER11$_{m\text{-}n}$.

Samples	Peak	q / Å^{-1}	q/q$_1$	Canonical Ratio	Deviation	FWHM / Å^{-1}	Amplitude / a.u.	Lattice parameter / nm	Phase structure
PLC11$_{25}$-*b*-PGMA$_{50}$	q$_1$	0.04959	1	1	\	0.013	4.7×10^{-3}	14.6	HEX-like
	q$_2$	0.09012	1.82	$\sqrt{3}$	+5.1%	0.034	7.2×10^{-5}		
	q$_3$	0.15219	3.07	3	+2.3%	0.019	3.6×10^{-5}		
PLC11$_{25}$-*b*-PGMA$_{25}$	q$_1$	0.05851	1	1	\	0.013	2.8×10^{-3}	10.7	LAM-like
	q$_2$	0.12255	2.10	2	+5.0%	0.022	7.2×10^{-5}		
	q$_3$	0.18086	3.09	3	+3.0%	0.011	6.8×10^{-6}		
PLC11$_{50}$-*b*-PGMA$_{50}$	q$_1$	0.04001	1	1	\	0.019	6.9×10^{-3}	15.6	LAM-like
	q$_2$	0.11318	2.83	3	-5.7%	0.053	4.2×10^{-4}		
	q$_3$	0.14912	3.73	4	-6.8%	0.014	1.2×10^{-5}		
PLC11$_{50}$-*b*-PGMA$_{25}$	q$_1$	0.05507	1	1	\	0.015	9.5×10^{-4}	13.2	Inverted HEX-like
	q$_2$	0.09315	1.69	$\sqrt{3}$	-2.4%	0.018	5.7×10^{-5}		
	q$_3$	0.13764	2.50	$\sqrt{7}$	-5.5%	0.016	1.3×10^{-5}		
B-ER11$_{25\text{-}50}$	q$_1$	0.04578	1	1	\	0.018	2.5×10^{-3}	15.8	HEX-like
	q$_2$	0.08362	1.83	$\sqrt{3}$	+5.4%	0.044	1.1×10^{-4}		
	q$_3$	0.1384	3.02	3	+0.8%	0.036	3.1×10^{-5}		

Table S8. SAXS peak positions for PLCx_m-*b*-PGMA$_n$ and B-ER11$_{m-n}$ (Continued).

Samples	Peak	q / Å^{-1}	q/q_1	Canonical Ratio	Deviation	FWHM / Å^{-1}	Amplitude / a.u.	Lattice parameter / nm	Phase structure
B-ER11$_{50-50}$	q_1	0.03017	1	1	\	0.019	6.7×10^{-3}	20.8	LAM-like
	q_2	0.09322	3.09	3	+3.0%	0.032	2.0×10^{-4}		
	q_3	0.12165	4.03	4	+0.8%	0.088	1.1×10^{-4}		
B-ER11$_{50-25}$	q_1	0.02584	1	1	\	0.026	3.9×10^{-3}	\	\
	q_2	\	\	\	\	\	\		
	q_3	0.13334	5.16	\	\	0.044	2.4×10^{-5}		

Determined based on the SAXS results. LAM-like: Lattice parameter = $2\pi/q_1$; HEX-like and inverted HEX-like: Lattice parameter = $4\pi/(\sqrt{3}q_1)$; FWHM: Full width at half maximum.

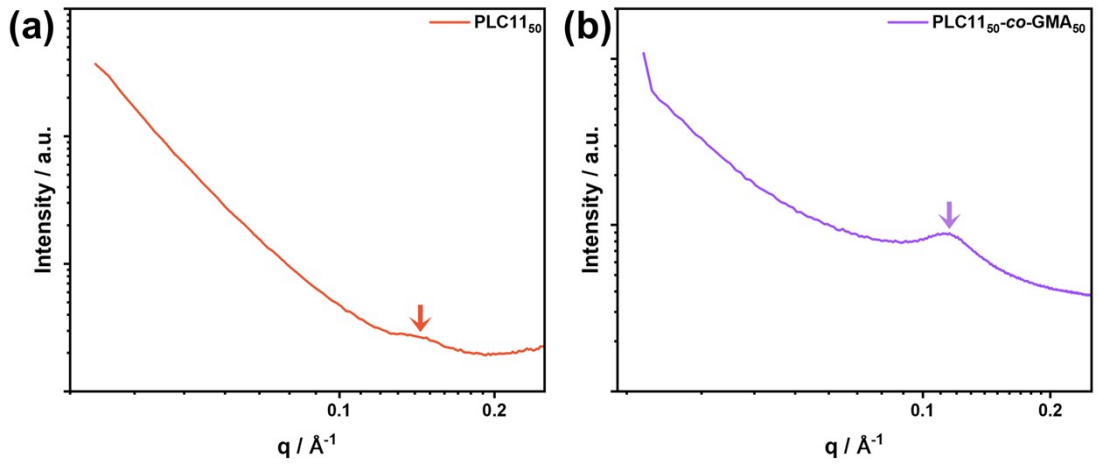

Fig. S22. SAXS curve of (a) PLC11$_{50}$ and (b) PLC11$_{50}$-*co*-PGMA$_{50}$.

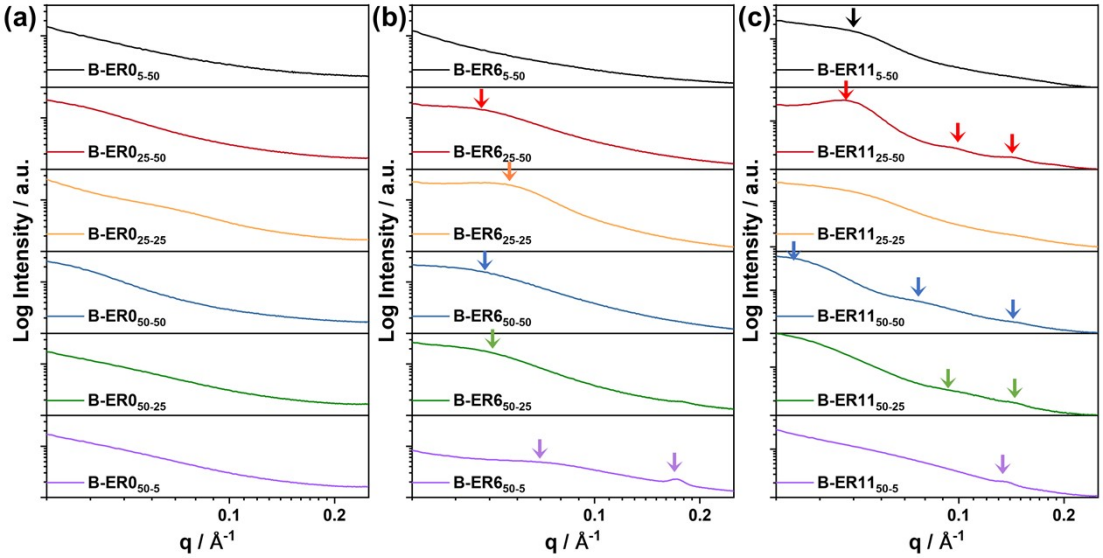

Fig. S23. SAXS curves of (a) B-ER0$_{m\text{-}n}$, (b) B-ER6$_{m\text{-}n}$, and (c) B-ER11$_{m\text{-}n}$.

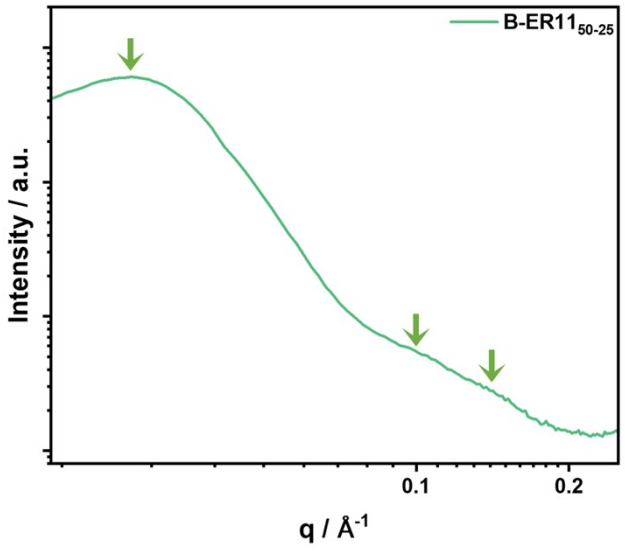

Fig. S24. SAXS curve of B-ER11$_{50\text{-}25}$ begining with a lower angle.

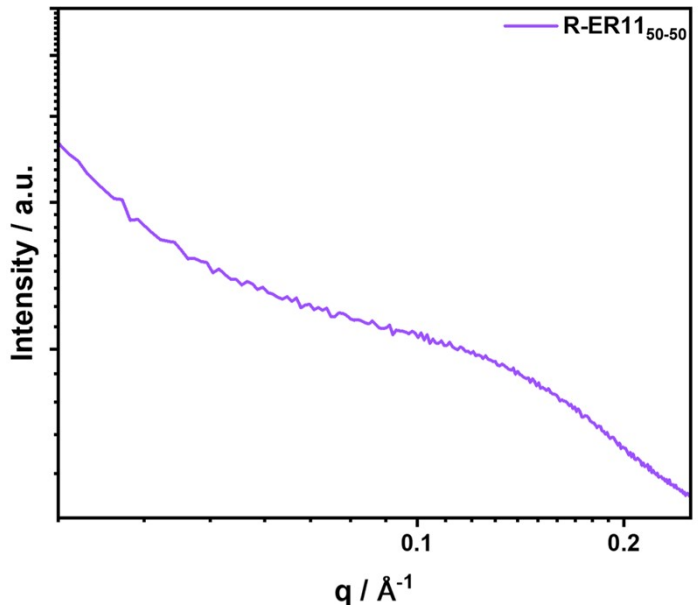

Fig. S25. SAXS curve of R-ER11$_{50-50}$.

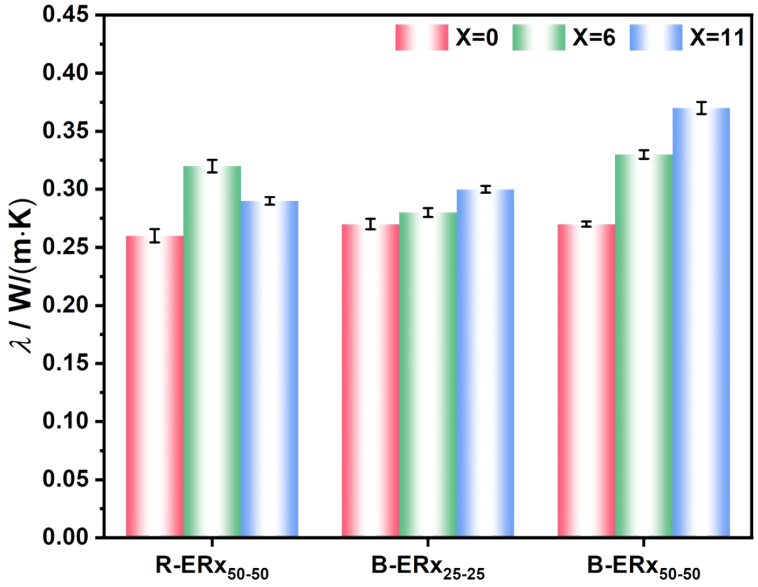

Fig. S26. The λ values of B-ERx$_{m-n}$ comparing with R-ERx$_{m-n}$.

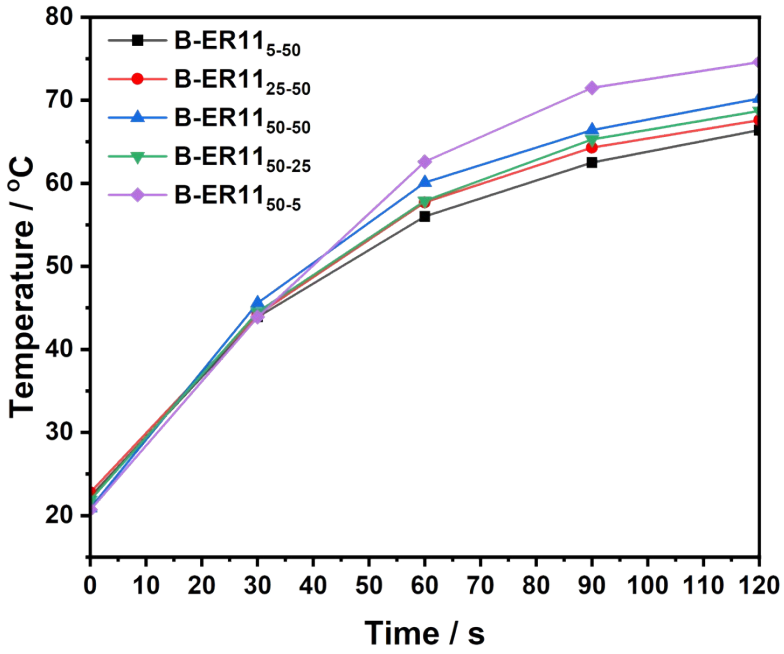

Fig. S27. Surface temperatures at different time for B-ER11$_{m-n}$